Long indium-rich InGaAs nanowires by SAG-HVPE

Emmanuel Chereau, Gabin Grégoire, Geoffrey Avit, Thierry Taliercio, Philipp Staudinger, Heinz Schmid, C. Bougerol, Agnès Trassoudaine, Evelyne Gil, Ray Lapierre, et al.

Long indium-rich InGaAs nanowires by SAG-HVPE

Emmanuel Chereau[1], Gabin Grégoire[1], Geoffrey Avit[1], Thierry Taliercio[2], Philipp Staudinger[3], Heinz Schmid[3], Catherine Bougerol[4], Agnès Trassoudaine[1], Evelyne Gil[1], Ray R. LaPierre[5], Yamina André[1]

[1]Université Clermont Auvergne, CNRS, Clermont Auvergne INP, Institut Pascal, F-63000 Clermont-Ferrand, France
[2]IES, Univ. Montpellier, CNRS, Montpellier F-34000, France
[3]IBM Research Europe - Zürich, Saumerstrasse 4, 8803 Rüschlikon, Switzerland
[4]Université Grenoble Alpes, CNRS, Institut Neel, 38000 Grenoble, France
[5]Department of Engineering Physics, McMaster University, Hamilton, Ontario Canada, L8S4L7

E-mail: emmanuel.chereau@uca.fr, evelyne.gil@uca.fr, yamina.andre@uca.fr

Abstract

We demonstrate the selective area growth (SAG) of InGaAs nanowires (NWs) on GaAs (111)B substrates using hydride vapor phase epitaxy (HVPE). A high growth rate of more than 50 µm/h and high aspect ratio NWs were obtained. Composition along the NWs was investigated by energy dispersive x-ray spectroscopy (EDS) giving an average indium composition of 84%. This is consistent with the composition of 78% estimated from the photoluminescence (PL) spectrum of the NWs. Crystal structure analysis of the NWs by transmission electron microscopy indicated random stacking faults related to zinc-blende/wurtzite (ZB/WZ) polytypism. This work demonstrates the ability of HVPE for growing high aspect ratio InGaAs NW arrays.

Introduction

III-V semiconductor nanowires (NWs) are currently considered as the most versatile family of one-dimensional (1-D) nanostructures due to their unique physical properties and potential applications in nanoelectronics and optoelectronics[1–3]. Among III-V semiconductors, a particular interest lies in the growth of InGaAs material because of its widely tunable bandgap wavelength (from 880 to

3500 nm) and high electron mobility. The composition of planar InGaAs heterostructures is restricted to nearly lattice-matched substrates, such as $In_{0.53}Ga_{0.47}As$ on InP[4], to inhibit strain induced defects. In contrast, the more efficient strain relaxation of NWs allows the integration of InGaAs NWs on diverse substrates with much larger composition tunability. Thus, a wide variety of applications have been realized using InGaAs NWs such as infrared photodetectors[5], lasers[6], field-effect transistors[7,8], and photovoltaics[9,10].

Several methods have been developed to grow InGaAs NWs. The most common one is the vapor-liquid-solid (VLS) method[11] where a metal catalyst is used to nucleate NWs. For example, a wide range of InGaAs composition has been obtained by Au-assisted growth[12,13]. However, Au may incorporate into NWs and cause deep level centers[14,15]. Consequently, much effort has been invested in growing Au-free InGaAs NWs in the self-catalyzed VLS approach, where the Au catalyst is replaced by a group III element droplet. Nevertheless, some issues exist with self-assisted growth, such as an incubation time for In precipitation and a limitation in In concentration (less than 5%)[16,17]. Therefore, efforts have been made to use a catalyst-free vapour-solid (VS) method to grow InGaAs NWs. In addition, to achieve homogeneous NW growth[18], selective area growth (SAG) is widely used. In SAG, the growth occurs in defined openings on a patterned dielectric mask. This leads to highly regular, large-scale NW arrays. SAG of InGaAs NWs has been demonstrated by MBE and MOVPE[19,20].

In this paper, we used hydride vapour phase epitaxy (HVPE) to grow InGaAs NWs. Using III-chloride and V-hydride precursors, HVPE has been proven to be a powerful tool to grow III-V materials. Thanks to the low sticking coefficient of the III-chloride precursors on dielectric masks[21], SAG with high selectivity has successfully used to grow binary GaAs and InAs on both GaAs (111)B and Si (111) substrates[22–24]. Here, we study the features of SAG of InGaAs NWs using SiO_x patterned GaAs (111)B substrate by HVPE. A remarkably high axial growth rate (more than 50 µm/h) leads to NWs with a high aspect ratio of 23. NW composition is investigated by energy dispersive X-ray spectroscopy (EDS) along the NWs. Crystal structures and optical properties of these NWs are also discussed.

Experimental

SAG of InGaAs NWs was carried out on GaAs (111)B substrates. The SiO_x dielectric mask was deposited by plasma-enhanced chemical vapor deposition (PECVD) and patterned by electron beam lithography into an array of holes. The hole diameter was 60 nm and the pitch was 2 µm. The sample was transferred in a hot-wall HVPE operating at atmospheric pressure. The reactor is divided into three zones (source zone, mixing zone and deposit zone) and is heated by a six zone split tube furnace. H_2 is used as a carrier gas. The GaCl and InCl precursors were formed in the source zone by reacting gaseous HCl with liquid gallium and indium at 760 °C. The AsH_3 gas was introduced in the mixing zone which is heated at a higher temperature to guarantee homogeneous mixing of the gas phase. When AsH_3 is introduced in the reactor, it is completely decomposed in As_2/As_4 gaseous species with equilibrium concentrations. The substrate was deposited in the deposit zone which is maintained at a lower temperature than the mixing zone. In this study, no intentional catalyst was used for growth. The vapor phase above the substrate is composed of GaCl, InCl, As_2/As_4, H_2 and residual HCl species. At the growth temperature used in this study, the partial pressure of As_4 is 100 times greater than that of As_2. The partial pressure of As_4, GaCl, and InCl are noted as P_{As4}, P_{GaCl}, and P_{InCl}, respectively. In this study, $P_{As4}=7.5\times10^{-4}$ atm, $P_{GaCl}=6.6\times10^{-4}$ atm, and $P_{InCl}=1\times10^{-2}$ atm leading to a $III_{In}/(III_{In}+III_{Ga})$ ratio of 0.94 and to a $(III_{In}+III_{Ga})/V$ ratio of 3.55. The substrate was stabilized under As_4 during the heating phase. The growth starts when InCl and GaCl fluxes are turned on simultaneously. The sample was heated at 715 °C for InGaAs deposition and the growth time was 10 min. At the end of the growth, both InCl and GaCl are turned off simultaneously. The substrate was then cooled under As_4 until the temperature of 560 °C.

The morphology of as-grown NWs was investigated using a scanning electron microscope (SEM) with an acceleration voltage of 3 kV and the crystal structure was studied using a FEI-TECNAI high resolution transmission electron microscopy (HRTEM) operated at an acceleration voltage of 200 kV. EDS was used in a SEM to estimate the chemical composition of the NWs based on K-alpha In and Ga lines. Photoluminescence (PL) spectroscopy was performed using a Brucker-Vertex 70 FTIR spectrometer equipped with a KBr beamsplitter and a cooled InSb detector. PL was excited by a 780 nm laser diode. The spot diameter was 200 µm and the power was 5 mW. The sample was cooled using a closed cycle He flow cryostat.

Results and discussion

Figure 1 shows SEM images of as-grown InGaAs NWs and three EDS profiles along a single NW. The SEM images in Figure 1a reveal pencil-like shaped NWs grown in the [111]B direction with a diameter of 370 nm at the top of the NW and a length of 8.7 µm, corresponding to a remarkable axial growth rate of more than 50 µm/h. This value is notable in SAG compared to the growth rate below 10 µm/h observed in MOVPE[25,26] and MBE[20,27]. The NW morphology is pencil-like because the intrinsic growth rate of the (111)B facet is greatly superior to the lateral facets assumed to be {-110}. The radial growth rate on the {-110} side facets, which consist of Ga-As rows, is generally very low over a wide range of HVPE conditions because of the low adsorption of GaCl on the {-110} surface[28]. However, it cannot be excluded that this morphology could also be interpreted by the formation of element III droplets at the top of InGaAs NWs which shrink at the end of growth.

Figure 1b-d shows EDS profiles along the length of a singles NW. The EDS results show an average In composition of 84%, highlighting that these NWs are In-rich InGaAs. The difference between the In composition in the vapor phase (93%) and the In composition in the solid (84%) is a well-known phenomenon for the growth of ternary NWs. This is mainly explained by the different transport of Ga and In atoms into the NW, due to the different diffusion lengths on the NW sidewalls and different desorption rates[29]. The Ga and In concentrations were nearly homogeneous along the length of the three different NWs analyzed. Such composition has already been demonstrated by MBE and MOVPE but on shorter NWs[20,30]. Therefore, HVPE seems to be a powerful tool, able to achieve ternary composition with good homogeneity over nearly 10 µm in NW length.

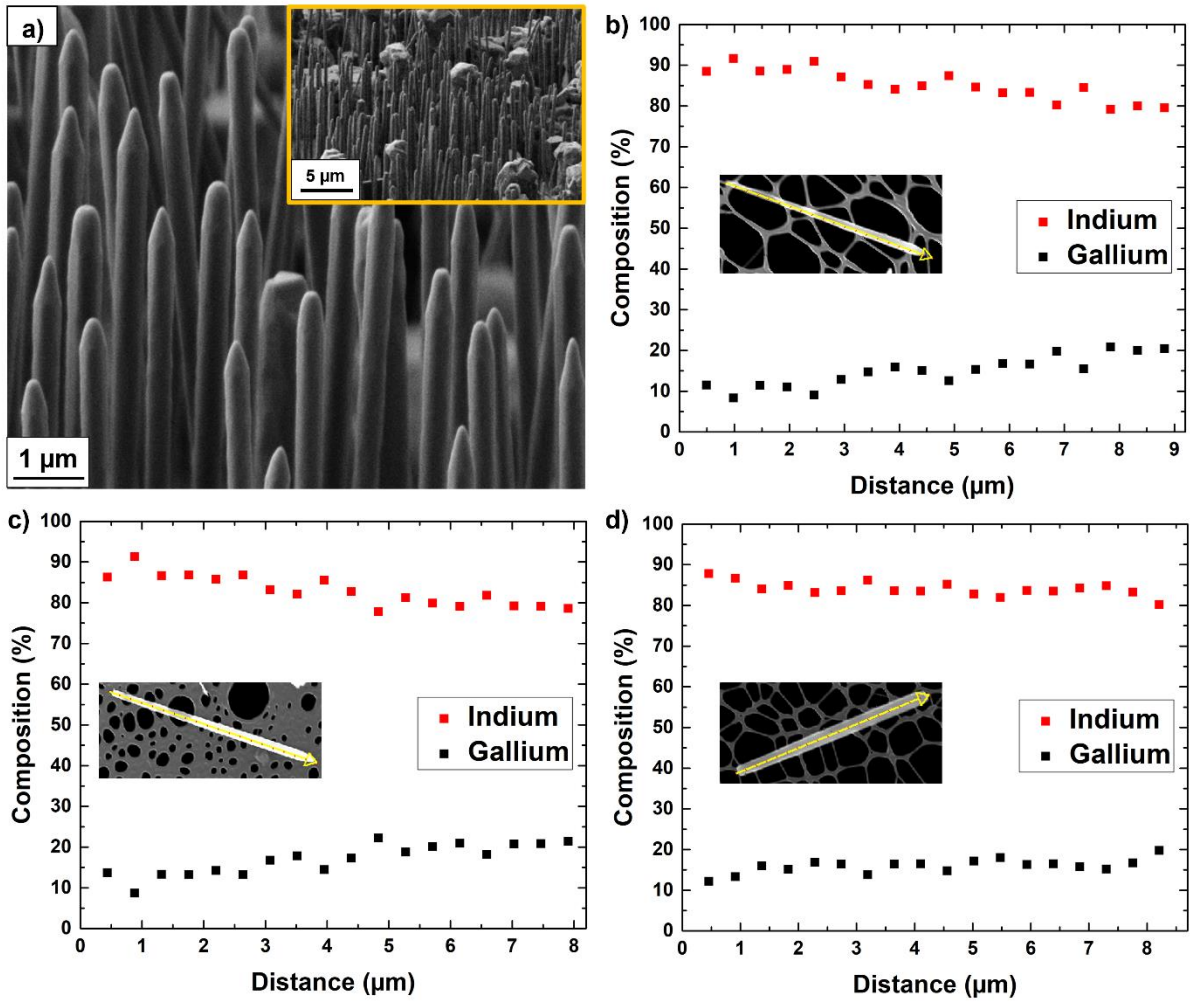

Figure 1: a) 20° tilted-view SEM image of InGaAs NWs with an inset that shows a wide field SEM image. EDS profiles along the [111]B direction of single InGaAs NWs showing an average indium composition of b) 85%, c) 83% and d) 84%. Points run from base to top of the NW.

The crystal structure of the NWs was characterized by HRTEM as shown in Figure 2. Random stacking faults related to the zinc-blende/wurtzite (ZB/WZ) polytypism are observed. This polytypism is commonly observed during the growth of III-As NWs along the [111]B direction[20,31,32] and is mainly due to the small difference in the internal formation energies of ZB and WZ phases[33–35].

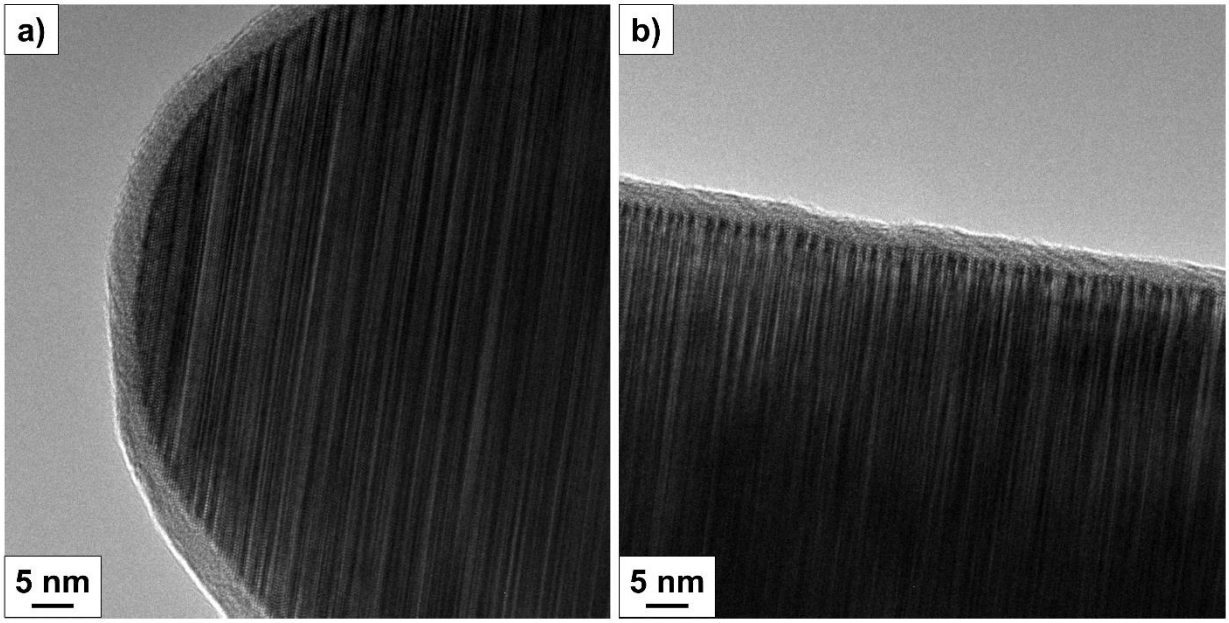

Figure 2: HRTEM images of InGaAs NW at a) the top and b) the bottom of the NW. The shell ~~present~~ visible on the NW is an oxide layer. The incident electron beam was along the ⟨1−10⟩ direction.

In order to confirm the composition, photoluminescence (PL) characterization was performed at low temperature (14 K) on as-grown NW array. The spectrum in Figure 3 shows a main broad peak at 0.58 eV with a secondary peak at 0.50 eV. The main peak is likely due to either a band-to-band or exciton-related transition and the low energy peak may be due to unintentional impurity-related transitions. The full width at half maximum (FWHM) of 0.042 eV of the main peak is similar to observations made on InGaAs NWs grown by MOVPE and MBE[18,19,36]. Two hypotheses could explain the width of the main emission peak. As TEM measurements have shown, the as-grown NWs exhibit a high density of stacking faults related to the ZB/WZ polytypism. Consequently, the presence of both ZB/WZ phases could result in an increase of the emission peak width due to difference in the bandgap energy of these two phases[18,37]. The second reason concerns the homogeneity of composition between the NWs. A variation of the composition leads to different energy emissions. To determine the composition from the main peak of the PL spectrum, Eq. (1) taken from Ref.[38] is used:

$$Eg(x,T) = 0.42 + 0.625x - \left[\frac{5.8}{(T+300)} - \frac{4.19}{(T+271)}\right].10^{-4}T^2x - \frac{4.19.10^{-4}T^2}{(T+271)} + 0.475x^2 \quad (1)$$

where E_g is the InGaAs bandgap in eV (taken as the peak energy of the PL main peak), x is the Ga composition and T is the absolute temperature. From Eq. (1), the indium composition is estimated at 78%. This is close to the indium composition of 84% measured by EDS. However, we note that Eq. (1) was verified for unstrained cubic ZB material. The NWs are expected to be unstrained due to their high aspect ratio but they exhibit a ZB/WZ polytypism. As a consequence, the WZ phase of InGaAs NWs may affect the position of the PL peak and therefore Eq. (1) does not provide the precise value of the composition.

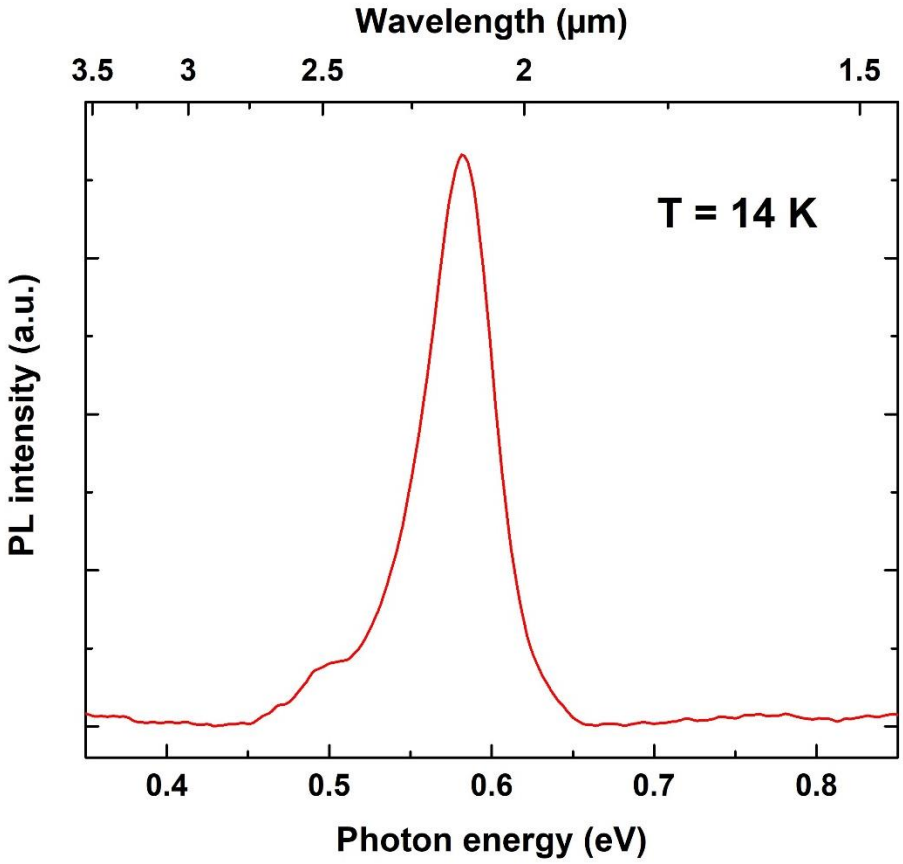

Figure 3: 14 K PL spectrum of InGaAs NW array.

Conclusion

In conclusion, we demonstrated the SAG of InGaAs NWs on GaAs (111)B substrate with good selectivity using the HVPE technique. A high growth rate was observed of more than 50 µm/h leading to high aspect ratio NWs. The TEM measurements confirmed the presence of stacking

faults in the NWs. The composition was investigated by EDS profiles along a single NW, resulting in an average indium composition of 84% with nearly homogeneous concentrations along the NW length. The estimated composition by PL of 78% is consistent with the EDS results. Overall, SAG of InGaAs NWs by HVPE provides a new platform for the fabrication of homogeneous InGaAs NW arrays with high aspect ratios.

Acknowledgements

This work was supported by Région Auvergne Rhône-Alpes; Pack ambition international NanoSpring DRV_PIP_2021-252_IP_NANOSPRING (https://www.auvergnerhonealpes.fr/77-logo.htm).

This work was supported by the International Research Center "Innovation Transportation and Production Systems" of the I-SITE CAP 20-25."

It was also funded by the program “Investissements d’avenir” of the French ANR agency, the French government IDEX-SITE initiative 16-µIDEX-0001 (CAP 20-25), the European Commission (Auvergne FEDER Funds), and the Region Auvergne in the framework of the LabEx IMobS3 (ANR-10-LABX-16-01).

The authors thank 2MAtech, Aubiere, France, for scanning electron microscopy measurements.

This work also received funding from the H2020 ERC POC project ENUF, grant number 790448.

RRL acknowledges the financial support of the Natural Sciences and Engineering Research Council of Canada from grants RGPIN-2018-04015.

References

(1) Barrigón, E.; Heurlin, M.; Bi, Z.; Monemar, B.; Samuelson, L. Synthesis and Applications of III–V Nanowires. *Chem. Rev.* **2019**, *119* (15), 9170–9220. https://doi.org/10.1021/acs.chemrev.9b00075.

(2) Zhang, Y.; Wu, J.; Aagesen, M.; Liu, H. III–V Nanowires and Nanowire Optoelectronic Devices. *J. Phys. Appl. Phys.* **2015**, *48* (46), 463001. https://doi.org/10.1088/0022-3727/48/46/463001.

(3) Tomioka, K.; Ikejiri, K.; Tanaka, T.; Motohisa, J.; Hara, S.; Hiruma, K.; Fukui, T. Selective-Area Growth of III-V Nanowires and Their Applications. *J. Mater. Res.* **2011**, *26* (17), 2127–2141. https://doi.org/10.1557/jmr.2011.103.
(4) Yerino, C. D.; Liang, B.; Huffaker, D. L.; Simmonds, P. J.; Lee, M. L. Review Article: Molecular Beam Epitaxy of Lattice-Matched InAlAs and InGaAs Layers on InP (111)A, (111)B, and (110). *J. Vac. Sci. Technol. B* **2017**, *35* (1), 010801. https://doi.org/10.1116/1.4972049.
(5) Tan, H.; Fan, C.; Ma, L.; Zhang, X.; Fan, P.; Yang, Y.; Hu, W.; Zhou, H.; Zhuang, X.; Zhu, X.; Pan, A. Single-Crystalline InGaAs Nanowires for Room-Temperature High-Performance Near-Infrared Photodetectors. *Nano-Micro Lett.* **2016**, *8* (1), 29–35. https://doi.org/10.1007/s40820-015-0058-0.
(6) Kim, H.; Lee, W.-J.; Farrell, A. C.; Morales, J. S. D.; Senanayake, P.; Prikhodko, S. V.; Ochalski, T. J.; Huffaker, D. L. Monolithic InGaAs Nanowire Array Lasers on Silicon-on-Insulator Operating at Room Temperature. *Nano Lett.* **2017**, *17* (6), 3465–3470. https://doi.org/10.1021/acs.nanolett.7b00384.
(7) Tomioka, K.; Yoshimura, M.; Fukui, T. A III–V Nanowire Channel on Silicon for High-Performance Vertical Transistors. *Nature* **2012**, *488* (7410), 189–192. https://doi.org/10.1038/nature11293.
(8) Tomioka, K.; Fukui, T. Current Increment of Tunnel Field-Effect Transistor Using InGaAs Nanowire/Si Heterojunction by Scaling of Channel Length. *Appl. Phys. Lett.* **2014**, *104* (7), 073507. https://doi.org/10.1063/1.4865921.
(9) Shin, J. C.; Kim, K. H.; Yu, K. J.; Hu, H.; Yin, L.; Ning, C.-Z.; Rogers, J. A.; Zuo, J.-M.; Li, X. InxGa1-xAs Nanowires on Silicon: One-Dimensional Heterogeneous Epitaxy, Bandgap Engineering, and Photovoltaics. *Nano Lett.* **2011**, *11* (11), 4831–4838. https://doi.org/10.1021/nl202676b.
(10) Chiba, K.; Yoshida, A.; Tomioka, K.; Motohisa, J. Vertical InGaAs Nanowire Array Photodiodes on Si. *ACS Photonics* **2019**, *6* (2), 260–264. https://doi.org/10.1021/acsphotonics.8b01089.
(11) Wagner, R. S.; Ellis, W. C. VAPOR-LIQUID-SOLID MECHANISM OF SINGLE CRYSTAL GROWTH. *Appl. Phys. Lett.* **2004**, *4* (5), 89–90. https://doi.org/10.1063/1.1753975.
(12) Wu, J.; Borg, B. M.; Jacobsson, D.; Dick, K. A.; Wernersson, L.-E. Control of Composition and Morphology in InGaAs Nanowires Grown by Metalorganic Vapor Phase Epitaxy. *J. Cryst. Growth* **2013**, *383*, 158–165. https://doi.org/10.1016/j.jcrysgro.2013.07.038.
(13) Jung, C. S.; Kim, H. S.; Jung, G. B.; Gong, K. J.; Cho, Y. J.; Jang, S. Y.; Kim, C. H.; Lee, C.-W.; Park, J. Composition and Phase Tuned InGaAs Alloy Nanowires. *J. Phys. Chem. C* **2011**, *115* (16), 7843–7850. https://doi.org/10.1021/jp2003276.
(14) Bar-Sadan, M.; Barthel, J.; Shtrikman, H.; Houben, L. Direct Imaging of Single Au Atoms Within GaAs Nanowires. *Nano Lett.* **2012**, *12* (5), 2352–2356. https://doi.org/10.1021/nl300314k.
(15) Breuer, S.; Pfüller, C.; Flissikowski, T.; Brandt, O.; Grahn, H. T.; Geelhaar, L.; Riechert, H. Suitability of Au- and Self-Assisted GaAs Nanowires for Optoelectronic Applications. *Nano Lett.* **2011**, *11* (3), 1276–1279. https://doi.org/10.1021/nl104316t.
(16) Heiß, M.; Gustafsson, A.; Conesa-Boj, S.; Peiró, F.; Morante, J. R.; Abstreiter, G.; Arbiol, J.; Samuelson, L.; Morral, A. F. i. Catalyst-Free Nanowires with Axial InxGa1−xAs/GaAs

Heterostructures. *Nanotechnology* **2009**, *20* (7), 075603. https://doi.org/10.1088/0957-4484/20/7/075603.
(17) Heiss, M.; Ketterer, B.; Uccelli, E.; Morante, J. R.; Arbiol, J.; Morral, A. F. i. In(Ga)As Quantum Dot Formation on Group-III Assisted Catalyst-Free InGaAs Nanowires. *Nanotechnology* **2011**, *22* (19), 195601. https://doi.org/10.1088/0957-4484/22/19/195601.
(18) Koblmüller, G.; Abstreiter, G. Growth and Properties of InGaAs Nanowires on Silicon. *Phys. Status Solidi RRL – Rapid Res. Lett.* **2014**, *8* (1), 11–30. https://doi.org/10.1002/pssr.201308207.
(19) Chiba, K.; Tomioka, K.; Yoshida, A.; Motohisa, J. Composition Controllability of InGaAs Nanowire Arrays in Selective Area Growth with Controlled Pitches on Si Platform. *AIP Adv.* **2017**, *7* (12), 125304. https://doi.org/10.1063/1.4993689.
(20) Treu, J.; Speckbacher, M.; Saller, K.; Morkötter, S.; Döblinger, M.; Xu, X.; Riedl, H.; Abstreiter, G.; Finley, J. J.; Koblmüller, G. Widely Tunable Alloy Composition and Crystal Structure in Catalyst-Free InGaAs Nanowire Arrays Grown by Selective Area Molecular Beam Epitaxy. *Appl. Phys. Lett.* **2016**, *108* (5), 053110. https://doi.org/10.1063/1.4941407.
(21) Gil, E.; André, Y.; Cadoret, R.; Trassoudaine, A. 2 - Hydride Vapor Phase Epitaxy for Current III–V and Nitride Semiconductor Compound Issues. In *Handbook of Crystal Growth (Second Edition)*; Kuech, T. F., Ed.; Handbook of Crystal Growth; North-Holland: Boston, 2015; pp 51–93. https://doi.org/10.1016/B978-0-444-63304-0.00002-0.
(22) Zeghouane, M.; Grégoire, G.; Chereau, E.; Avit, G.; Staudinger, P.; Moselund, K. E.; Schmid, H.; Coulon, P.-M.; Shields, P.; Isik Goktas, N.; LaPierre, R. R.; Trassoudaine, A.; André, Y.; Gil, E. Selective Area Growth of GaAs Nanowires and Microplatelet Arrays on Silicon by Hydride Vapor-Phase Epitaxy. *Cryst. Growth Des.* **2023**. https://doi.org/10.1021/acs.cgd.2c01105.
(23) Grégoire, G.; Zeghouane, M.; Goosney, C.; Goktas, N. I.; Staudinger, P.; Schmid, H.; Moselund, K. E.; Taliercio, T.; Tournié, E.; Trassoudaine, A.; Gil, E.; LaPierre, R. R.; André, Y. Selective Area Growth by Hydride Vapor Phase Epitaxy and Optical Properties of InAs Nanowire Arrays. *Cryst. Growth Des.* **2021**, *21* (9), 5158–5163. https://doi.org/10.1021/acs.cgd.1c00518.
(24) Chereau, E.; Dubrovskii, V. G.; Grégoire, G.; Avit, G.; Staudinger, P.; Schmid, H.; Bougerol, C.; Coulon, P.-M.; Shields, P. A.; Trassoudaine, A.; Gil, E.; LaPierre, R. R.; André, Y. Importance of As and Ga Balance in Achieving Long GaAs Nanowires by Selective Area Epitaxy. *Cryst. Growth Des.* **2023**, *23* (6), 4401–4409. https://doi.org/10.1021/acs.cgd.3c00172.
(25) Azimi, Z.; Gopakumar, A.; Ameruddin, A. S.; Li, L.; Truong, T.; Nguyen, H. T.; Tan, H. H.; Jagadish, C.; Wong-Leung, J. Tuning the Crystal Structure and Optical Properties of Selective Area Grown InGaAs Nanowires. *Nano Res.* **2022**, *15* (4), 3695–3703. https://doi.org/10.1007/s12274-021-3914-x.
(26) Kohashi, Y.; Sakita, S.; Hara, S.; Motohisa, J. Pitch-Independent Realization of 30-Nm-Diameter InGaAs Nanowire Arrays by Two-Step Growth Method in Selective-Area Metalorganic Vapor-Phase Epitaxy. *Appl. Phys. Express* **2013**, *6* (2), 025502. https://doi.org/10.7567/APEX.6.025502.

(27) Treu, J.; Xu, X.; Ott, K.; Saller, K.; Abstreiter, G.; Finley, J. J.; Koblmüller, G. Optical Absorption of Composition-Tunable InGaAs Nanowire Arrays. *Nanotechnology* **2019**, *30* (49), 495703. https://doi.org/10.1088/1361-6528/ab3ef7.
(28) Gil-Lafon, E.; Napierala, J.; Castelluci, D.; Pimpinelli, A.; Cadoret, R.; Gérard, B. Selective Growth of GaAs by HVPE: Keys for Accurate Control of the Growth Morphologies. *J. Cryst. Growth* **2001**, *222* (3), 482–496. https://doi.org/10.1016/S0022-0248(00)00961-1.
(29) Dubrovskii, V. G.; Leshchenko, E. D. Kinetically Controlled Composition of III-V Ternary Nanostructures. *Phys. Rev. Mater.* **2023**, *7* (5), 056001. https://doi.org/10.1103/PhysRevMaterials.7.056001.
(30) Chiba, K.; Tomioka, K.; Yoshida, A.; Motohisa, J. Composition Controllability of InGaAs Nanowire Arrays in Selective Area Growth with Controlled Pitches on Si Platform. *AIP Adv.* **2017**, *7* (12), 125304. https://doi.org/10.1063/1.4993689.
(31) Wu, J.; Borg, B. M.; Jacobsson, D.; Dick, K. A.; Wernersson, L.-E. Control of Composition and Morphology in InGaAs Nanowires Grown by Metalorganic Vapor Phase Epitaxy. *J. Cryst. Growth* **2013**, *383*, 158–165. https://doi.org/10.1016/j.jcrysgro.2013.07.038.
(32) Shin, J. C.; Choi, K. J.; Kim, D. Y.; Choi, W. J.; Li, X. Characteristics of Strain-Induced InxGa1–xAs Nanowires Grown on Si(111) Substrates. *Cryst. Growth Des.* **2012**, *12* (6), 2994–2998. https://doi.org/10.1021/cg300210h.
(33) Cantoro, M.; Brammertz, G.; Richard, O.; Bender, H.; Clemente, F.; Leys, M.; Degroote, S.; Caymax, M.; Heyns, M.; Gendt, S. D. Controlled III/V Nanowire Growth by Selective-Area Vapor-Phase Epitaxy. *J. Electrochem. Soc.* **2009**, *156* (11), H860. https://doi.org/10.1149/1.3222852.
(34) Caroff, P.; Dick, K. A.; Johansson, J.; Messing, M. E.; Deppert, K.; Samuelson, L. Controlled Polytypic and Twin-Plane Superlattices in Iii–v Nanowires. *Nat. Nanotechnol.* **2009**, *4* (1), 50–55. https://doi.org/10.1038/nnano.2008.359.
(35) Dubrovskii, V. G.; Sibirev, N. V. Growth Thermodynamics of Nanowires and Its Application to Polytypism of Zinc Blende III-V Nanowires. *Phys. Rev. B* **2008**, *77* (3), 035414. https://doi.org/10.1103/PhysRevB.77.035414.
(36) Dubrovskii, V. G.; Reznik, R. R.; Kryzhanovskaya, N. V.; Shtrom, I. V.; Ubyivovk, E. D.; Soshnikov, I. P.; Cirlin, G. E. MBE-Grown InxGa1 –xAs Nanowires with 50% Composition. *Semiconductors* **2020**, *54* (6), 650–653. https://doi.org/10.1134/S1063782620060056.
(37) Morkötter, S.; Funk, S.; Liang, M.; Döblinger, M.; Hertenberger, S.; Treu, J.; Rudolph, D.; Yadav, A.; Becker, J.; Bichler, M.; Scarpa, G.; Lugli, P.; Zardo, I.; Finley, J. J.; Abstreiter, G.; Koblmüller, G. Role of Microstructure on Optical Properties in High-Uniformity In${}_{1\ensuremath{-}x}$Ga${}_{x}$As Nanowire Arrays: Evidence of a Wider Wurtzite Band Gap. *Phys. Rev. B* **2013**, *87* (20), 205303. https://doi.org/10.1103/PhysRevB.87.205303.
(38) Paul, S.; Roy, J. B.; Basu, P. K. Empirical Expressions for the Alloy Composition and Temperature Dependence of the Band Gap and Intrinsic Carrier Density in GaxIn1−xAs. *J. Appl. Phys.* **1991**, *69* (2), 827–829. https://doi.org/10.1063/1.348919.